Annual variations of physical properties of desert dust over Israel

P. L. Israelevich, E. Ganor, Z. Levin, and J. H. Joseph

Department of Geophysics and Planetary Sciences, The Raymond and Beverly Sackler Faculty of Exact Sciences,
Tel Aviv University, Ramat Aviv, Israel

[1]   The annual variation of the desert dust aerosol loading above the eastern Mediterranean is studied. Three periods are identified, March–May, July–August, and September–November, for which the properties of dust particles are distinctly different. The dust layers are at higher altitudes and consist of larger particles in summer and autumn than in spring. The real part of the refractive index of the particles is the same for summer and autumn periods and exceeds the real part of the refractive index measured during the spring. The imaginary part of the refractive index is negligible both in spring and in summer, whereas the imaginary refractive index becomes significant in September–November, indicating the presence of absorbing aerosols. The difference is attributed to different sources and desert dust trajectories in these periods. In spring the desert aerosol from the source in Chad is transported to the eastern Mediterranean predominantly along the North African coast. This is the motion associated with Sharav cyclones. The aerosols come to the eastern Mediterranean via Egypt from the sources near the Red Sea in July–August. In autumn the dust arrives to the eastern Mediterranean from the Libyan coast.   *INDEX TERMS:* 0305 Atmospheric Composition and Structure: Aerosols and particles (0345, 4801); 0322 Atmospheric Composition and Structure: Constituent sources and sinks; 0368 Atmospheric Composition and Structure: Troposphere—constituent transport and chemistry; 1640 Global Change: Remote sensing; 4801 Oceanography: Biological and Chemical: Aerosols (0305); *KEYWORDS:* desert dust, dust transport, dust sources, aerosol properties

1. Introduction

[2]   The Mediterranean region is strongly affected by the presence of desert dust from the largest global source of desert aerosol: the North African Deserts. The aerosol affects the atmosphere both directly by changing reflection and absorption of the solar radiation and indirectly by influencing cloud albedo, precipitation development and cloud lifetime [*Levin et al.*, 1996; *Wurzler et al.*, 2000; *Yin et al.*, 2002; *Rosenfeld et al.*, 2001]. Therefore systematic measurements of the aerosol distributions are necessary for climate studies, rain formation and weather prediction. The seasonal aerosol activity in the Mediterranean was studied in numerous papers [e.g., *Manes and Joseph*, 1971; *Joseph et al.*, 1973; *Joseph and Wolfson*, 1975; *Yaalon and Ganor*, 1979; *Joseph*, 1984; *Koren et al.*, 2001; *Levin and Lindberg*, 1979; *Levin et al.*, 1980; *Bergametti et al.*, 1989; *Dayan et al.*, 1991; *Alpert and Ganor*, 1993, 2001; *Molinaroli et al.*, 1993; *Kubilay and Saydam*, 1995; *Loye-Pilot and Martin*, 1996; *Marticorena and Bergametti*, 1996; *Moulin et al.*, 1997, 1998; *Prospero et al.*, 2002; *Israelevich et al.*, 2002] and can be outlined as follows. Three major configurations of Saharan dust trans-

port over the Mediterranean Sea were identified by *Moulin et al.* [1998]. In spring the dust is brought to the eastern Mediterranean by Sharav cyclones [*Alpert and Ziv*, 1989] traveling eastward along the North African coast. In summer, the main aerosol activity is observed in the Central Mediterranean. At the end of the summer-early autumn, low pressures near the Balearic Islands result in dust transport predominantly to the western Mediterranean. Using TOMS aerosol index distributions, *Israelevich et al.* [2002] have shown that in the spring-summer months dust sources in Northern Africa dominate over sinks, and, hence, a significant amount of desert dust is always present in the atmosphere even in the days when there is no direct mobilization of the dust from the primary sources. This last conclusion is in agreement with the measurements of *Levin and Lindberg* [1979], who observed dust to be always present in the atmosphere over Israel. Thus the dust is transported to the Mediterranean each time when the appropriate meteorological conditions (primarily Sharav cyclones) arise. If a proper transport configuration occurs during the time of strong dust supply from the primary source, then the desert dust intrusion in the Mediterranean region takes the form of spectacular storm-like events. Clouds of desert aerosol particles take the shape of giant plumes that can span the north-south extent of the Mediterranean and are often separated from the surface. During the dust storms, the total
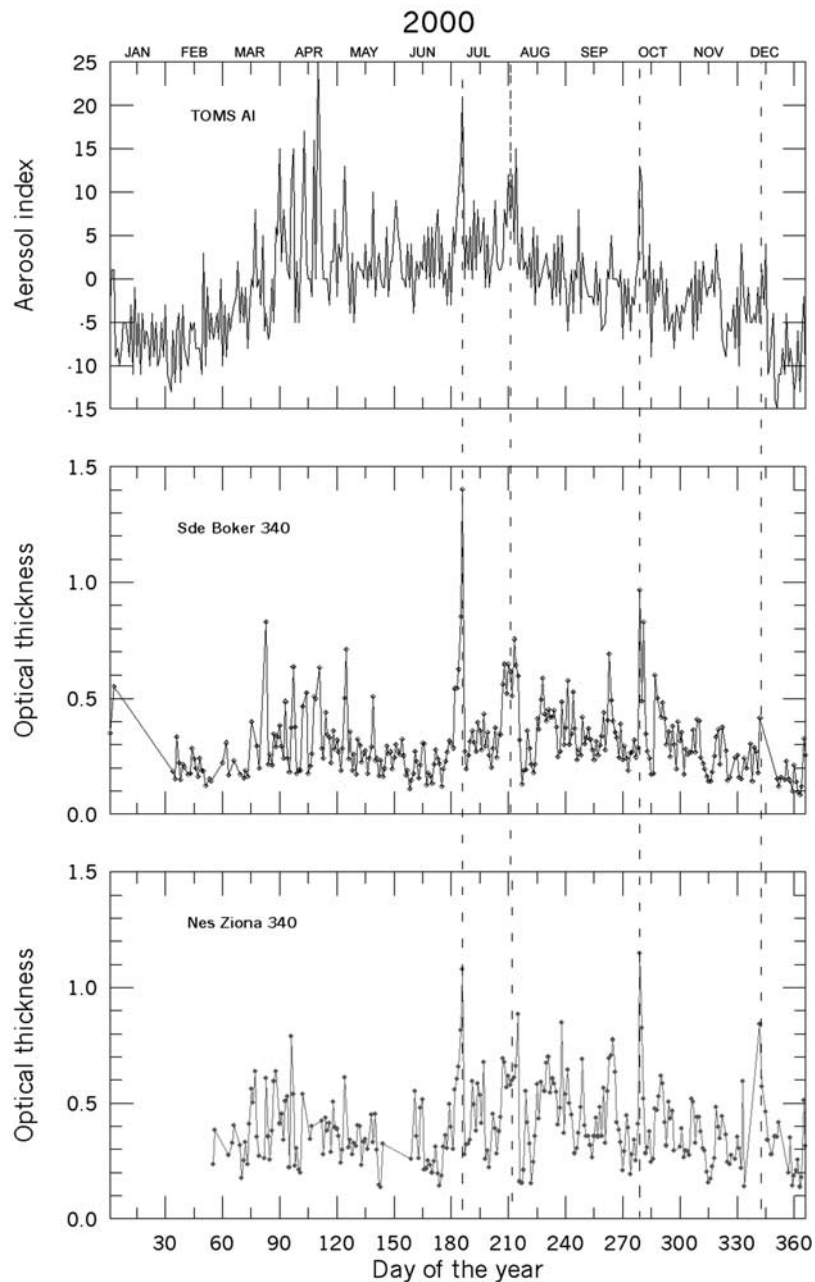
Figure 1. Dust episodes in the year 2000: (top) values of the TOMS aerosol index above Israel; (middle) aerosol optical thickness as measured by AERONET station in Sde Boker; (bottom) aerosol optical thickness observed in Ness Ziona.

optical depth in the visible solar spectrum is more than one and may, occasionally, reach values as high as 6. Identifiable dust plumes appear first in the Western sector of the sea, and then move eastward with the speed of ~7–8 degrees/day [*Israelevich et al.*, 2002, Figure 8], corresponding to the average motion of the Sharav cyclone. In spring this motion continues at least up to the eastern coast of the sea. In summer, the dust plumes do not penetrate longitudes east of ~15°.

[3] The above scheme describes an average seasonal dynamics of regional aerosol loading. Specific dust storms may exhibit different dynamics, and routine daily observations are required in order to obtain regional and local

aerosol budgets. These observations are provided by two complementary instruments: a set of AERONET stations measuring, in particular, dust spectral optical thickness and by satellite (e.g., Earth Probe, Terra, Acqua and SeaWifs) observations of desert dust radiance. Combination of these two independent data sources is necessary, first of all for the following reason. Whereas ground based stations provide, in an ideal case, continuous time series of local data, their spatial coverage of regions of interest is not uniform and far from being complete. On the other hand, the space data at the same point on the Earth's surface are obtained, usually, once a day and do not provide necessary time resolution of the events. Recently a comprehensive study of ground-
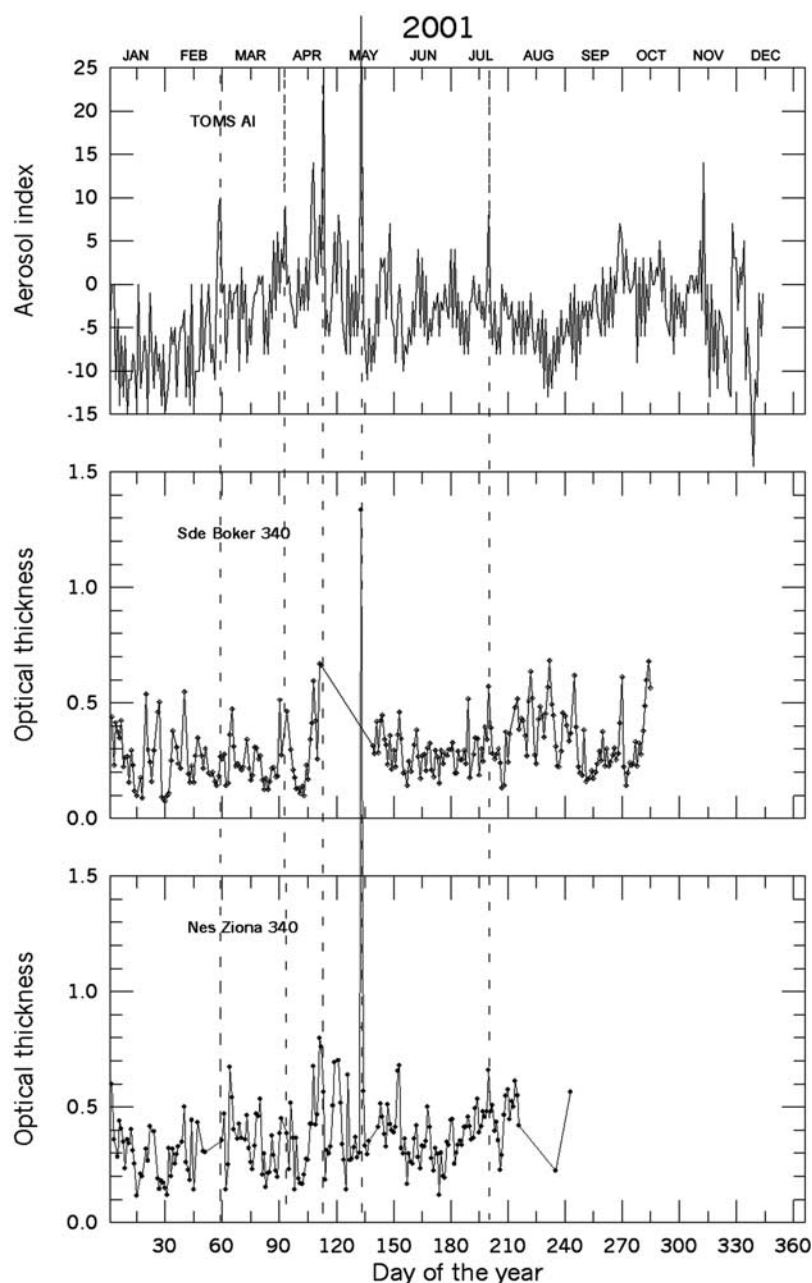
Figure 2. Same as in Figure 1, but for the year 2001.

based and space data of local dust dynamics have been undertaken by *Sabbah et al.* [2001] who derived the full cycle of dust activity in the Alexandria region of the eastern Mediterranean. In the present paper, we study the annual climatology of the desert dust in Israel using the TOMS aerosol index and the aerosol optical thickness as measured by AERONET stations.

2. Data Set

[4] We use the data on the desert dust optical thickness from two AERONET stations located in Israel. Ness Ziona (NZ) station is located at 31°55′N, 34°47′E, and the data are available starting in February 2000. Another station is in Sde Boker (SB) (30°51′N, 34°45′E) and provides data since

January 1996. The distance between the two stations is 120 km. Sun photometers established at these stations provide the aerosol optical thickness τ_λ at wavelengths $\lambda = 340, 380, 440, 500, 670, 870,$ and 1020 nm (for certain periods measurements in the 500 nm channel are absent in SB). We use data for τ_λ along with dust particles size distribution and aerosol refractive index obtained by the inversion procedure developed by *Dubovik and King* [2000] available at http://aeronet.gsfc.nasa.gov.

[5] The TOMS aerosol index (AI) [*Herman et al.*, 1997] from the Earth Probe satellite is available since August 1996. It is defined as

$$AI = -100\left\{\log\left[(I_A/I_B)_{mes}\right] - \log\left[(I_A/I_B)_{mod}\right]\right\}$$
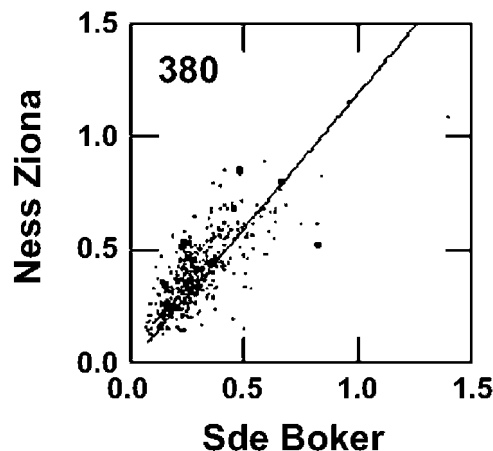
Figure 3. Aerosol optical thickness at 380 nm measured in Ness Ziona versus the same measurements in Sde Boker.

(where the indices *mes* and *mod* refer to the measured and modeled for pure Raleigh scattering, respectively). The aerosol index is positive for absorbing aerosols (e.g., dust and smoke particles) and negative for non-absorbing aerosols (e.g., sulfates) [*Herman et al.*, 1997; *Torres et al.*, 1998]. Moreover, for clouds, $AI \approx 0$ [*Herman et al.*, 1997], and therefore the main effect of the sub pixel clouds on the aerosol index is the partial screening of the aerosol. The aerosol index is proportional to the single- scattering co-albedo and to the absorption optical depth (i.e., to the amount of the aerosol present in the column along the line of sight). However, it also exhibits strong dependence on the height distribution of the aerosols. In particular, this dependence may make it very difficult to detect the aerosol presence at altitudes below 1 km by the UV spectral contrast method when the main part of a heavy dust fall is close to the surface. In spite of that, the TOMS aerosol index is an effective measure of the dust loading in the atmosphere, and it has been successfully used to determine the dynamics of

global distributions of the absorbing aerosols [*Herman et al.*, 1997] and their sources [*Prospero et al.*, 2002].

[6] We use the AI for the pixel with coordinates 32.5N, 34.375 E. The period starting in January 1996 and ending in December 2001 is covered in this study.
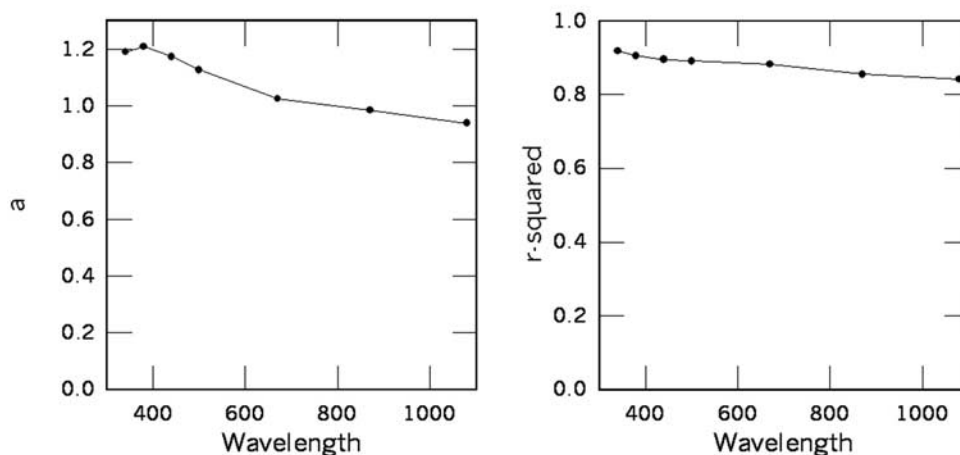
3. Results

[7] Figures 1 and 2 show aerosol index (upper panels) and aerosol optical depths at 340 nm as measured in NZ (middle panels) and SB (lower panels). These graphs correspond well to the general scheme outlined above: most of the dust activity is observed in spring and summer-autumn, the lowest activity is in winter.

[8] Independent data sets correspond well to each other. The larger the optical depth measured by AERONET stations, the higher is the aerosol index. The days of dust storms are also clearly seen in all three sets, vertical dashed lines mark some of them. One can see some peaks in January–February, which means that minor dust storms may occur even in winter.

[9] Before we proceed with more detailed study of annual variation of the dust properties, it would be instructive to investigate the correlation between the τ_λ values obtained in NZ and SB. Optical depths measured in NZ and SB correlate very well. Figure 3 shows the optical thickness measured in NZ versus SB data for $\lambda = 380$ nm. The straight line shows the best fits passing through the origin ($\tau_{NS} = a \cdot \tau_{SB}$). The dependence on wavelength $a(\lambda)$ and the correlation coefficient are shown in Figure 4. Whereas a exhibits a slight decrease from 1.2 for 340 nm to less than 1 for 1020 nm, the correlation remains high and almost independent of wavelength. Thus on the spatial scale of 120 km (distance between NZ and SB) the aerosol loading of the atmosphere does not change significantly during a large-scale dust storm.

[10] Now, let us consider the average annual behavior of the aerosol optical thickness above the eastern Mediterranean. Using the data from NS and SB AERONET stations

Figure 4. Wavelength dependence of the correlation of the aerosol optical thickness measured in Ness Ziona and Sde Boker.
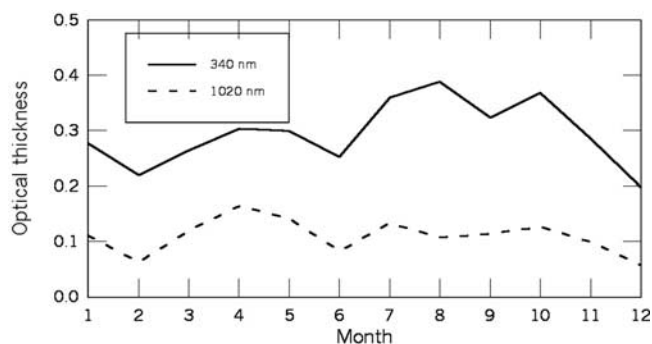
Figure 5. Annual variation of monthly averaged values of the aerosol optical thickness at 340 nm (solid line) and 1020 nm (dashed line).

we calculated the average values of the aerosol thickness for each month of the year. The results for τ_{1020} and τ_{340} are shown in Figure 5. In accordance with the general scheme outlined above, the optical depth reaches its maximal values in spring (March–May) and in late summer-early autumn (August–November). The smallest values are observed in winter, and additional minimum in aerosol optical thickness occurs in summer (June), when Sharav cyclones cannot reach the eastern Mediterranean coast. The comparison between average τ_{1020} and τ_{340} profiles show significant difference between spring and autumn events. The optical

depths at the 1020 nm wavelength are largest in spring, whereas data of the 340 nm channels exhibit larger thickness during autumn events. In other the words, the ratio τ_{1020}/τ_{340} varies systematically during the year indicating annual changes in the size distribution and/or chemical composition of desert dust arriving to Israel.

[11] The distribution of the aerosol optical thickness above Israel shown in Figure 5 differs significantly from the annual variation of dust episodes derived by *Ganor* [1994] from a 33 year cycle of observation (1958–1991). The *Ganor* [1994] records show that the probability for a dust event increases from autumn to winter, remains steady during most of the winter, rises to a peak in April, and, in contrast to the present results, decreases sharply in summer. Whereas it is possible, in principle, that a change in annual variation occurred between the years (1958–1991) and (1996–2001), the most plausible explanation of this discrepancy is as follows. The measurements of suspended dust, analyzed by *Ganor* [1994], were performed near the Earth surface, whereas the AERONET data used for the present study provide the aerosol amount in the whole atmospheric column, at all altitudes. Therefore we can conclude that in July November the dust layer is at higher altitudes than in March–May.

[12] We calculated distributions of normalized optical thickness $\tau_\lambda^0 = \tau_\lambda/\tau_{340}$ and their monthly averages for the whole period of observations. The top panel of Figure 6 shows the annual distribution of τ_λ^0 as a two dimensional
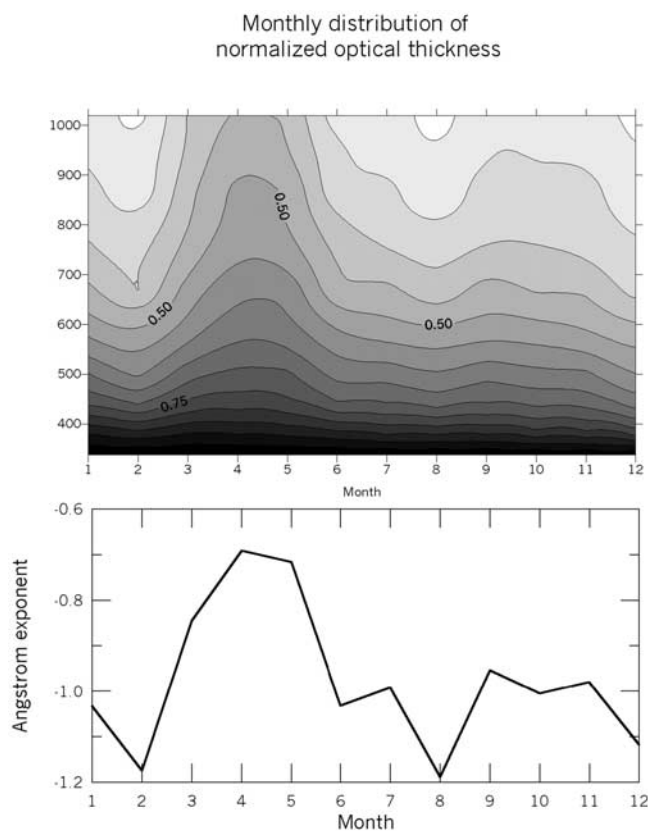
Figure 6. (top) Annual variation of the wavelength dependence of the normalized optical thickness $\tau_\lambda^0 = \tau_\lambda/\tau_{340}$. (bottom) Annual variation of Angstrøm exponent.
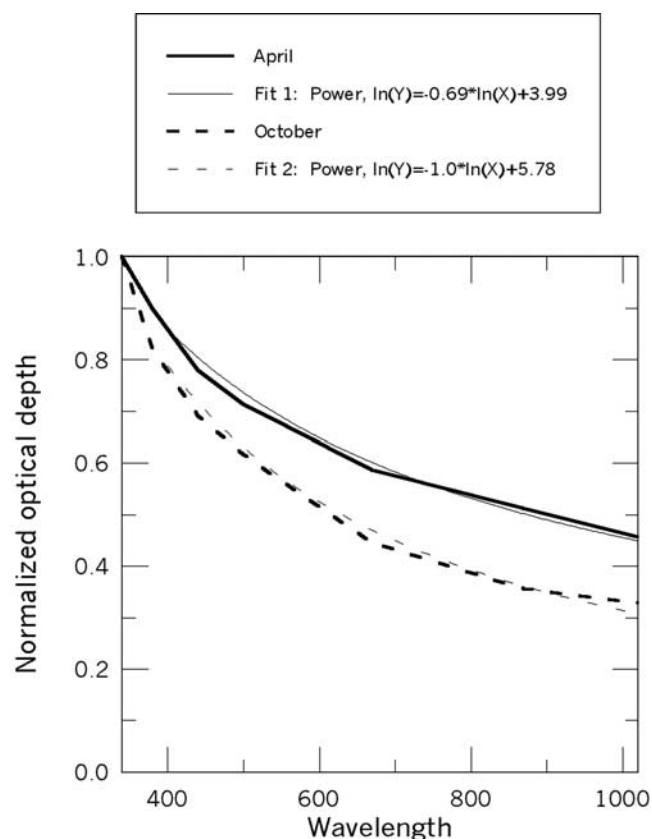
Figure 7. Dependencies of normalized optical thickness on the wavelength for April (solid line) and October (dashed lines). Thin lines show the best fits.
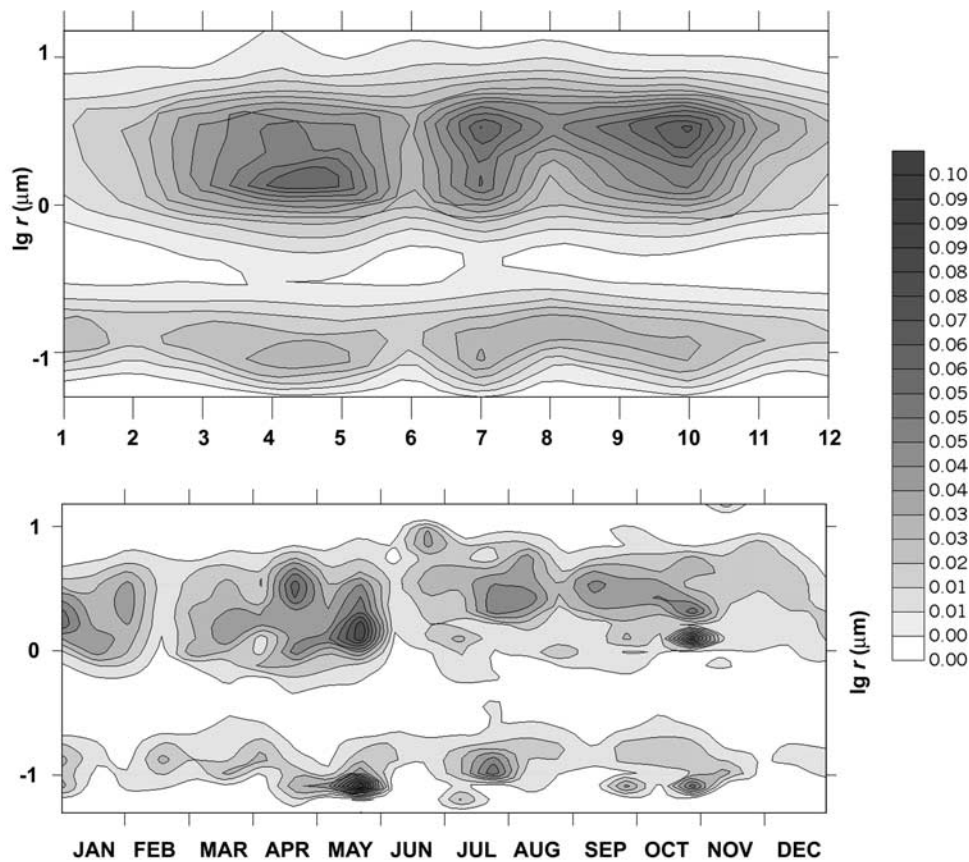
Figure 8. Annual variation of particle size distribution. Abscissa gives the month of the year, ordinate corresponds to the log *r*. Top panel corresponds to the size distributions averaged over the month; bottom panel is plotted for individual distributions.
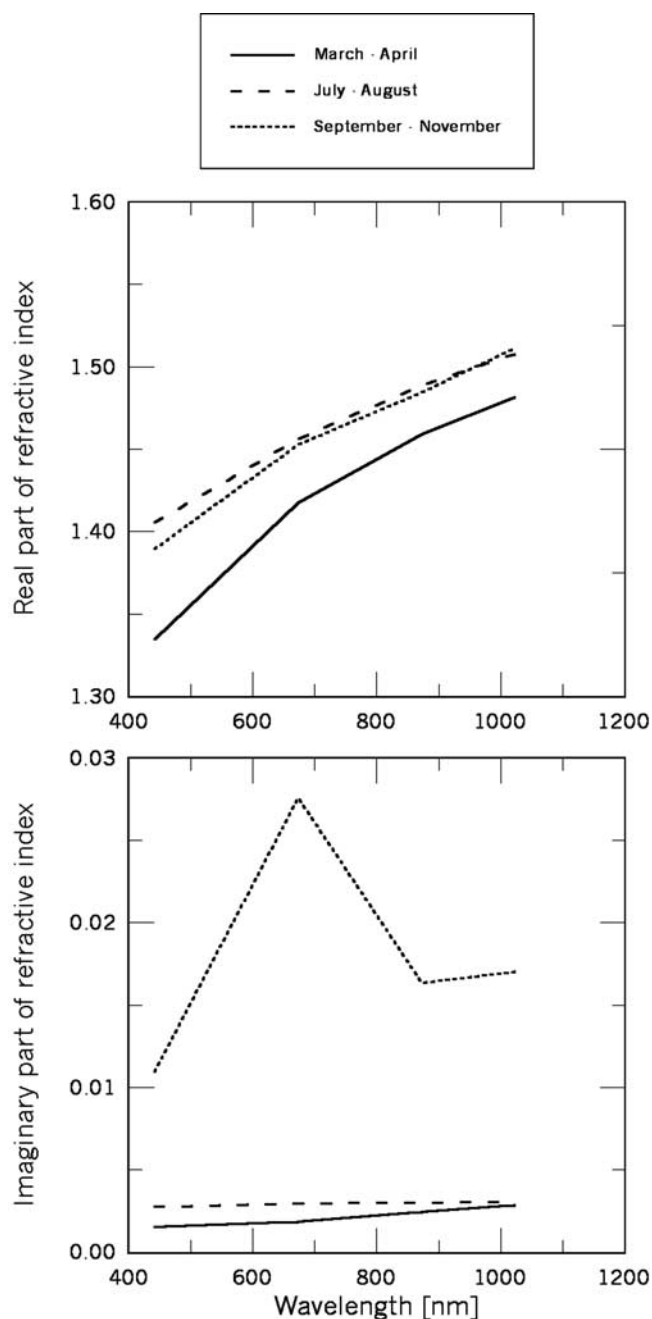
plot: abscissa is the month of the year, ordinate gives the wavelength and gray shadowing shows the corresponding value of normalized optical thickness. This presentation immediately reveals differences between spring and summer-autumn aerosols, with high values of optical thickness in all wavelengths in spring and a lower peak in autumn. The annual behavior of the Angstrørm exponent shown in the bottom panel confirms this difference. Figure 7 shows the normalized τ_λ^0 for April and October. In spring, normalized optical thickness is proportional to $\lambda^{-0.69}$, and to λ^{-1} in autumn.

[13] There is no doubt that the variations in aerosol optical thickness dependence on wavelength reflect changes in particle physico-chemical properties and their size distribution. Size distributions were obtained from the AERONET solar photometers data using the inversion procedure proposed by *Dubovik and King* [2000]. Figure 8 (top) shows the annual variation of size distributions averaged over a month of a year. Three different periods can be easily identified, spring (March–May), summer (July–August), and autumn (September–November). During these periods, size distributions exhibit the existence of both fine and coarse modes, but the size of coarse mode particles in summer-autumn is twice larger than in spring ($\sim$3 μm versus $\sim$1.5 μm). There is also some increase of the fine mode particles in autumn ($\sim$0.15 μm) as compared with their size in spring and summer ($\sim$0.09 μm).

[14] The aerosol fine mode seen in Figure 8 could be attributed to anthropogenic sources of pollution which are generated locally or transported from far away [*Levin et al.*, 1996; *Lelieveld et al.*, 2002]. The presence of the fine mode could be responsible for the relatively high negative values of the Angstrøm exponent.

[15] It is worth noting that averaging of size distributions over time intervals is a somewhat risky procedure, which tends to smooth the distributions and reduces their variations. However, in our case, the annual variability of individual size distributions (Figure 8, bottom) corresponds fairly well to the monthly averaged distributions behavior discussed above. The additional maximum in January which can be seen in the bottom panel is produced by a single size distribution obtained on 2 January 2001 and is not representative. Therefore we can conclude that the size distributions do not change significantly on a timescale of less than a month.

[16] Physical properties of particles are also different for these three distinct periods thus indicating changes in chemical composition. Figure 9 shows the average refractive index dependence on the wavelength for spring, summer and autumn. The top panel shows the real part of the refractive index $n(\lambda)$. Particles in summer and autumn have almost the same n which differs significantly from the real part of refractive index of the aerosols particles in spring. In contrast, the imaginary part of the refractive index enables

trajectories, or both. In order to find the trajectories of the aerosols we use the same approach as used by *Israelevich et al.* [2002]. Namely, we plot the distribution of largest aerosol index values observed at any given point of the geographical grid during the period 1996–2001. Since the largest values of *AI* occur along the main trajectories of dust motion, such distributions may be used in order to visualize the latter. These distributions are shown in Figure 10 (from top to bottom: March–May, July–August, and September–November). Black dots show source regions of the desert dust in Sahara, as determined by *Israelevich et al.* [2002] (*A* (Ahaggar and Tibesti near the Chad basin) and *B* (Eljouf
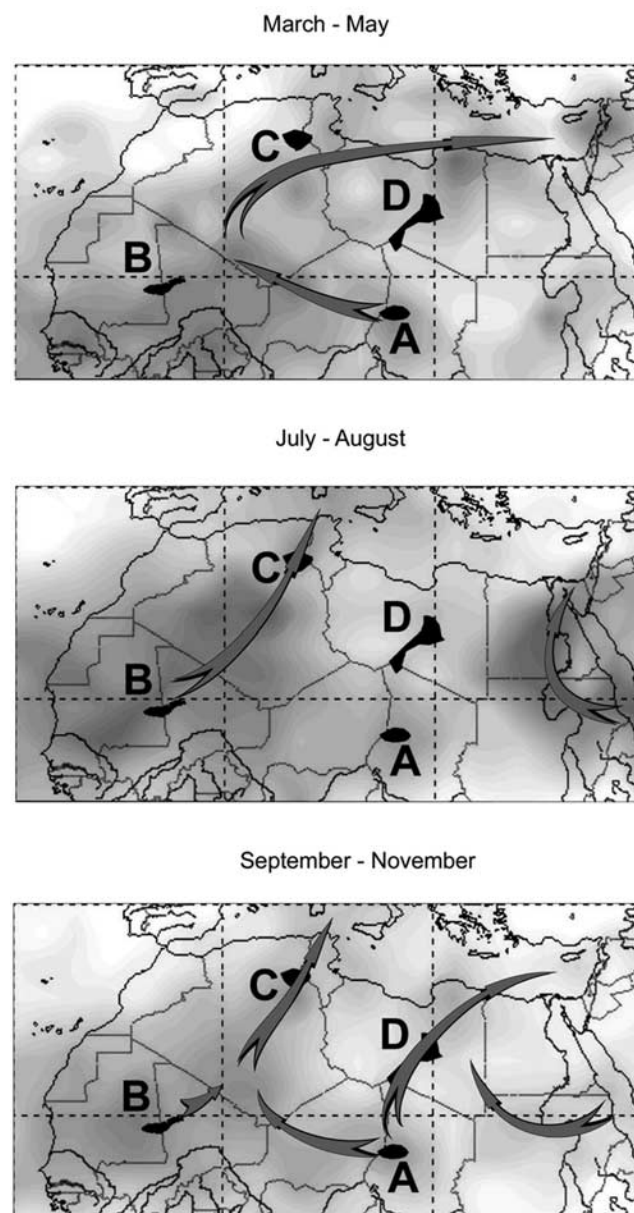

Figure 9. Dependence of (top) real and (bottom) imaginary parts of the refractive index. Solid, dashed, and dotted lines correspond to spring, summer and autumn, respectively.

one to distinguish between the summer and autumn aerosols. Whereas in summer, as in spring, *k* is small (non-absorbing aerosols), the imaginary part of the refractive index increases significantly in autumn. Of course, the wavelength dependence $k(\lambda)$ shown in Figure 9 is not realistic, and, presumably, is a consequence of the particles' non-sphericity [*Dubovik and King*, 2000], but it is clear that the imaginary part of refractive index is large in autumn indicating the presence of absorbing aerosols.

[17] The difference in physico-chemical properties of aerosol particles transported to the eastern Mediterranean may be due to different sources of the particles, different

Figure 10. Distribution of largest aerosol index values observed at any given point above North Africa and Mediterranean. Black areas denote main dust sources. Arrows show schematically the trajectories of the dust transport. From top to bottom: data for March–May, July–August, and September–November. See color version of this figure in the HTML.

basin) are the major sources). Arrows show schematically the dominating trajectories of dust storms. The geographical distributions differ significantly. In spring the desert aerosol from the source A in Chad and, maybe, from the source B, is transported to the eastern Mediterranean predominantly along the North African coast. This is the motion associated with Sharav cyclones as described above. The distribution for the summer months (July and August) shows a quite different transport scheme. Desert dust arrives from Saharan sources to the Western and Central Mediterranean, but does not propagate eastward. Instead, the aerosols in the eastern Mediterranean come via Egypt from the sources near the Red Sea (there are sources on both the African and Arabian coasts of the Red Sea). Therefore, indeed, the dust observed over Israel in spring and in summer originates from different sources.

[18] The distribution of maximal AI values for September–November is compatible with the dust trajectories determined by *Ganor and Foner* [1996]. It allows several different interpretations. The dust comes to the eastern Mediterranean coast from the Libyan coast. There are visualized trajectories of dust to the northeast of the Libyan coast from the Chad source (A), from the nearby Red Sea sources, and from the Libyan source (D). Moreover, trajectories in the autumn months pass over the geographically small but rather powerful source near Benghazi (31°N, 21°E). For lack of data on the flux of dust in the different regions, it is difficult to estimate the relative role of these possible sources for autumn aerosols above Israel.

4. Conclusion

[19] The annual variation of the dust aerosol above Israel exhibits three distinctly different periods of strong aerosol loading, March–May, July–August, and September–November. The dust distributions during these characteristic periods differ by size of the particles, their composition, and the height distribution of the aerosol layer. The particles are, generally, larger in summer and autumn periods, than in spring. The real part of the refractive index of the particles is the same for summer and autumn periods and exceeds the real part of the refractive index measured during the spring. On the other hand, both in spring and in summer, the imaginary part of the refractive index is negligible whereas in September–November, the imaginary refractive index becomes significant indicating the presence of absorbing aerosols. The heights of the dust layer are higher in summer and autumn than in spring.

References

Alpert, P., and E. Ganor, A jet stream associated heavy dust storm in the Western Mediterranean, *J. Geophys. Res.*, 98, 7339–7349, 1993.

Alpert, P., and E. Ganor, Sahara mineral dust measurements from TOMS: Comparison to surface observations over the Middle East for the extreme dust storm, March 14–17, 1998, *J. Geophys. Res.*, 106, 18,275–18,286, 2001.

Alpert, P., and B. Ziv, The Sharav cyclone: Observation and some theoretical considerations, *J. Geophys. Res.*, 94, 18,495–18,514, 1989.

Bergametti, G., A.-L. Dutot, P. Buat-Menard, R. Losno, and E. Remoudaki, Seasonal variability of the elemental composition of atmospheric aerosol over the northwestern Mediterranean, *Tellus, Ser. B*, 41, 353, 1989.

Dayan, U., J. L. Heffter, J. M. Miller, and G. Gutman, Dust intrusion events into the Mediterranean basin, *J. Appl. Meteorol.*, 30, 1185–1199, 1991.

Dubovik, O., and M. D. King, A flexible inversion algorithm for retrieval of aerosol optical properties from Sun and sky radiance measurements, *J. Geophys. Res.*, 105, 20,673–20,696, 2000.

Ganor, E., The frequency of Saharan dust episodes over Tel Aviv, Israel, *Atmos. Environ.*, 28, 2867–2871, 1994.

Ganor, E., and H. A. Foner, The mineralogical and chemical properties and the behavior of aeolian Saharan dust over Israel, in *The Impact of Desert Dust Across the Mediterranean*, edited by S. Guerzoni and R. Chester, pp. 163–172, Kluwer Acad, Norwell, Mass., 1996.

Herman, J. R., P. K. Bhartia, O. Torres, C. Hsu, C. Seftor, and E. Celarier, Global distributions of UV-absorbing aerosols from Nimbus 7/TOMS data, *J. Geophys. Res.*, 102, 16,911–16,922, 1997.

Israelevich, P. L., Z. Levin, J. H. Joseph, and E. Ganor, Desert aerosol transport in the Mediterranean region as inferred from the TOMS aerosol index, *J. Geophys. Res.*, 107(D21), 4572, doi:10.1029/2001JD002011, 2002.

Joseph, J. H., The sensitivity of a numerical model of the global atmosphere to the presence of a desert aerosol, in *Aerosols and Their Climatic Effects*, pp. 215–226, A. Deepak, Hampton, Va., 1984.

Joseph, J. H., and N. Wolfson, The ratio of absorption to back-scatter of solar radiation during Khamsin conditions and effects on the radiation balance, *J. Appl. Meteorol.*, 14, 1389–1396, 1975.

Joseph, J. H., A. Manes, and D. Ashbel, Desert aerosols transported by Khamsinic depressions and their climatic effects, *J. Appl. Meteorol.*, 12, 792–797, 1973.

Koren, I., E. Ganor, and J. H. Joseph, On the relation between size and shape of desert dust aerosol, *J. Geophys. Res.*, 106, 18,047–18,054, 2001.

Kubilay, N., and A. C. Saydam, Trace elements in atmospheric particulates over the eastern Mediterranean: Concentrations, sources, and temporal variability, *Atmos. Environ.*, 29, 2289–2300, 1995.

Lelieveld, J., et al., Global air pollution crossroads over the Mediterranean, *Science*, 298, 794–799, 2002.

Levin, Z., and J. D. Lindberg, Size distribution, chemical composition and optical properties of urban and desert aerosols in Israel, *J. Geophys. Res.*, 84, 6941–6950, 1979.

Levin, Z., J. H. Joseph, and Y. Mekler, Properties of Sharav (Khamsin) dust: Comparison of optical and direct sampling data, *J. Atmos. Sci.*, 37, 882–891, 1980.

Levin, Z., E. Ganor, and V. Gladstein, The effects of desert particles coated with sulfate on rain formation in the eastern Mediterranean, *J. Appl. Meteorol.*, 35, 1511–1523, 1996.

Loye-Pilot, M. D., and J. M. Martin, Saharan dust input to the western Mediterranean: An eleven years record in Corsica, in *The Impact of Desert Dust Across the Mediterranean*, edited by S. Guerzoni and R. Chester, pp. 191–200, Kluwer Acad., Norwell, Mass., 1996.

Manes, A., and J. H. Joseph, Secular and seasonal variations of the atmospheric turbidity in Israel at Jerusalem, *J. Appl. Meteorol.*, 10, 487–492, 1971.

Marticorena, B., and G. Bergametti, Two-year simulations of seasonal and interannual changes of the Saharan dust emissions, *Geophys. Res. Lett.*, 23(15), 1921–1924, 1996.

Molinaroli, E., S. Guerzoni, and G. Rampazzo, Contribution of the Saharan dust to the central Mediterranean basin, *Geol. Soc. Am. Bull.*, 284, 303–312, 1993.

Moulin, C., F. Guillard, F. Dulac, and C. E. Lambert, Long-term daily monitoring of Saharan dust load over ocean using Meteosat ISCCP-B2 data: 1. Methodology and preliminary results for 1983–1994 in the Mediterranean, *J. Geophys. Res.*, 102, 16,947–16,958, 1997.

Moulin, C., et al., Satellite climatology of African dust transport in Mediterranean atmosphere, *J. Geophys. Res.*, 103, 13,137–13,144, 1998.

Prospero, J. M., P. Ginoux, O. Torres, and S. E. Nicholson, Environmental characterization of global sources of atmospheric soil dust derived from the Nimbus 7 Total Ozone Mapping Spectrometer (TOMS) absorbing aerosol product, *Rev. Geophys.*, 40(1), 1002, doi:10.1029/2000RG000095, 2002.

Rosenfeld, D., Y. Rudich, and R. Lahav, Desert dust suppressing precipitation: A possible desertification feedback loop, *Proc. Natl. Acad. Sci. U. S. A.*, 98, 5975–5980, 2001.

Sabbah, I., C. Ichoku, Y. J. Kaufman, and L. Remer, Full tear cycle of desert dust spectral optical thickness and precipitable water vapor over Alexandria, Egypt, *J. Geophys. Res.*, 106, 18,305–18,316, 2001.

Torres, O., P. K. Bhartia, J. R. Herman, and Z. Ahmad, Derivation of aerosol properties from satellite measurements of backscattered ultravio-

let radiation: Theoretical basis, *J. Geophys. Res.*, *103*, 17,099–17,110, 1998.

Wurzler, S., T. G. Reisin, and Z. Levin, Modification of mineral dust particles by cloud processing and subsequent effects on drop size distributions, *J. Geophys. Res.*, *105*, 4501–4512, 2000.

Yaalon, D. H., and E. Ganor, East Mediterranean trajectories of dust-carrying storms from the Sahara and Sinai, in *Saharan Dust: Mobilization, Transport, Deposition*, edited by C. Morales, pp. 187–193, John Wiley, New York, 1979.

Yin, Y., S. Wurzler, Z. Levin, and T. Reisin, Interactions of mineral dust particles and clouds: Effects on precipitation and cloud optical properties, *J. Geophys. Res.*, *107*(D23), 4724, doi:10.1029/2001JD001544, 2002.

———————————

E. Ganor, P. L. Israelevich, J. H. Joseph, and Z. Levin, Department of Geophysics and Planetary Sciences, The Raymond and Beverly Sackler Faculty of Exact Sciences, Tel Aviv University, Ramat Aviv 69978, Israel. (peter@jupiter1.tau.ac.il)